

Fe-Ni alloy/polyamide 6 nanocomposites: effect of nanocrystalline metal particles on the mechanical and physical properties of the polymer

Marwa Mohamed · Azza El-Maghraby ·
Mona Abd EL-Latif · Hassan Farag ·
Kyriaki Kalaitzidou

Received: 30 July 2012 / Accepted: 28 March 2013 / Published online: 9 May 2013
© Springer Science+Business Media Dordrecht 2013

Abstract The focus of this study is to explore the potential use of Fe₄₀Ni₆₀/Polyamide 6 (PA6) nanocomposites in engineering applications by providing understanding of how the nanocrystalline (nc) metallic particles are altering physical properties of the polymer and the corresponding reinforcing mechanisms. This is the first study using nc Fe-Ni alloy, which has unique various properties, as a filler for polymers. nc Fe₄₀Ni₆₀ particles were chemically synthesized. The composites with various nanofiller loadings were made by compounding the materials, either by melt mixing (MM) or via solution mixing (SM), and injection molding. The results show that SM composites have remarkable mechanical and thermomechanical properties, but MM ones exhibit deteriorated properties. In addition, morphological and crystalline structure analyses indicate that there is good interfacial interaction between nanofiller and polymer only in SM composites. This is because the ferromagnetism of Fe-Ni alloy could be only overcome by intensive compounding. It is concluded that there

are four competing factors determining the overall performance of SM composites: i) degree of agglomeration and particle distribution within PA6 matrix and physical structural changes that occurred in PA6 due to presence of alloy particles including ii) crystallinity; iii) ratio of γ -form to α -form crystals; and iv) Glass transition temperature (T_g) of PA6. Overall, compared to other conventional nanoreinforcements for PA6, nc Fe-Ni alloy shows great promise and can lead to a new class of metal-polymer nanocomposites.

Keywords Nanocrystalline Fe-Ni alloy · Polymer nanocomposites · Mechanical properties · Morphology · Crystal structures · Structure–property relationship

Introduction

Recently, the fabrication of polymer nanocomposites (PNCs) has become a key technology for both engineering and advanced composite materials. The attention to nano-size fillers is due to their extremely high surface area that facilitates strong filler-polymer interactions even at low nano-filler loading, leading to significant improvements in material properties [1]. Numerous studies have shown that addition of nano-size metals to polymers can lead to a significant enhancement of many properties, such as stiffness, strength and hardness [2, 3], thermal stability and fire retardancy [4, 5], magnetic, optical, and electrical properties [6, 7]. All these make metal reinforced PNCs potential candidates for a wide variety of engineering applications including catalysis [8], chemical sensing [9], biomedical applications [10], electronics, photonics and for fabrication of electromagnetic [11] and optical [12] devices.

M. Mohamed · K. Kalaitzidou
The George W. Woodruff School of Mechanical Engineering,
Georgia Institute of Technology, Atlanta, GA 30332-0405, USA

M. Mohamed (✉) · A. El-Maghraby · M. Abd EL-Latif
Fabrication Technology Department, Institute of Advanced
Technology and New Materials, City of Scientific Research
and Technological Applications, New Borg El-Arab,
Alexandria 21934, Egypt
e-mail: mmohamed@mucsat.sci.eg

M. Mohamed
e-mail: marwa945@yahoo.com

H. Farag
Department of Chemical Engineering, Faculty of Engineering,
Alexandria University, Alexandria 21544, Egypt

Nanocrystalline Fe-Ni (nc Fe-Ni) alloys have been widely studied because of their high-saturation magnetization, low coercivity, good anticorrosion properties [13], low thermal expansion and excellent mechanical properties [14]. The studies focus on the synthesis of nc Fe-Ni alloys and the investigation of their magnetic and mechanical properties [13–15], without exploring the potential of using these alloys as nano-fillers in polymers.

Polyamide 6 (PA6) is a semicrystalline thermoplastic having a complicated polymorphic structure that exhibits two major crystal forms, namely α and γ . The α form crystals are more ordered, thermodynamically stable [16, 17] and stronger [18] than the metastable γ -form crystals. PA6 is extensively used in a number of consumer goods and industrial applications owing to its durability and high heat, wear and chemical resistance. Typical applications include fishing nets, brush bristles, fluid reservoirs and automotive components [19, 20].

The goal of this study is to explore the potential of using nc Fe₄₀Ni₆₀ as reinforcement for PA6 in order to provide new metal-PNC for engineering applications. This will be accomplished by developing Fe₄₀Ni₆₀/PA6 nanocomposites and characterizing their properties. Focus will be given on the alteration of PA6's physical properties due to the presence of metallic nanofiller and the mechanical and thermomechanical properties of the nanocomposites. nc Fe-Ni alloy is a supermagnetic material, so the nanoparticles have a great tendency to agglomerate and proper compounding methods need to be employed to eliminate or minimize the agglomeration. The nc Fe₄₀Ni₆₀ fine particles were synthesized by chemical reduction in aqueous solution and the Fe₄₀Ni₆₀/PA6 nanocomposites were prepared by compounding, either via direct melt mixing (MM) or solution mixing (SM), followed by injection molding. MM is simple, economical and therefore has a great potential in the commercial production of PNCs. On the other hand, SM is more effective route for the preparation of PNCs with remarkable properties [21].

Experimental

Materials

The chemicals used for the synthesis of nc Fe₄₀Ni₆₀ alloy were nickel chloride hexahydrate (NiCl₂·6H₂O, 98 %) and ferrous chloride (FeCl₂, 99 %) as sources of metal ions; hydrazine hydrate (N₂H₄·H₂O, 99 %) as a reducing agent, sodium hydroxide (NaOH, 99 %) as a catalyst and distilled water as a solvent. NiCl₂·6H₂O and N₂H₄·H₂O were purchased from Panreac Quimica, Spain. FeCl₂ and NaOH were obtained from Spectrum Chemical MFG. CORP, USA and El Nasr Pharmaceutical, Egypt, respectively. The polymer used was PA6 pellets (BX3WQ662[X] (ISO)) kindly supplied in sealed packages by Custom Resins, Inc, USA.

Formic acid (HCO₂H, 98 %) and ethanol (C₂H₅OH, 96 %) used as a solvent and a precipitant for PA6, respectively, were purchased from VWR, USA.

Synthesis of nc Fe₄₀Ni₆₀ particles

The synthesis of the nc Fe₄₀Ni₆₀ particles was done according to the protocol reported in our previous work [13]. Briefly, FeCl₂ and NiCl₂·6H₂O were dissolved in distilled water to form aqueous solution of 0.6 M with a [Fe²⁺]/[Ni²⁺] ratio of 4:6. The solution was vigorously stirred and heated to 80 °C. Then, a second solution of aqueous hydrazine, N₂H₄·H₂O, (50 wt%), and aqueous NaOH (0.1 M) was added to it. Fine black particles were precipitated as a result of the reduction reaction. The resulting particles were separated magnetically, washed repeatedly with distilled water until neutral pH and dried in vacuum at 35 °C for 2 days.

Preparation of Fe₄₀Ni₆₀/PA6 nanocomposites

The composites were made in a two step process: First the alloy particles were compounded with PA6 pellets either via MM or SM. The compounding was then followed by injection molding and standard Izod bars (ASTM D256) with nano-filler loading up to 5 wt% were fabricated. Before compounding, PA6 pellets were dried in a vacuum oven at 80 °C for 48 h. After molding, the specimens were sealed and placed in a desiccator for a minimum of 24 h prior to testing. The detailed sample codes are shown in Table 1.

A DSM Xplore 15 cc micro-compounder (vertical, co-rotating twin-screw extruder) and 10 cc micro-injection molding machine were used for the compounding and fabrication of MM nanocomposites, respectively. The conditions used were: 240 °C as T_{barrel} in the compounder and injection molding machine, screw speed of 150 rpm, T_{mold} of 70 °C and injection pressure of 0.76 MPa.

The solution mixed nanocomposites were prepared as follows. PA6 pellets were dissolved in formic acid at ambient temperature using magnetic stirring. The polymer

Table 1 Sample codes

Sample	Code
Manually mixed composites	
Control PA6	MM0
1 wt% Fe ₄₀ Ni ₆₀ / PA6	MM1
3 wt% Fe ₄₀ Ni ₆₀ / PA6	MM3
5 wt% Fe ₄₀ Ni ₆₀ / PA6	MM5
Solution mixed composites	
Control PA6	SM0
1 wt% Fe ₄₀ Ni ₆₀ / PA6	SM1
3 wt% Fe ₄₀ Ni ₆₀ / PA6	SM3
5 wt% Fe ₄₀ Ni ₆₀ / PA6	SM5

concentration in the solution was 10 wt%. The Fe₄₀Ni₆₀ particles were then added to the polymer solution and the mixture was vigorously stirred for 30 min. Addition of ethanol, with the ethanol/formic acid ratio being 2:1 vol/vol, initiated the precipitation of PA6 after 30 min and led to formation of the composite powder which was completed within 20 min. The composite powder was separated from mixed solvent through filtration and dried in vacuum oven at 80 °C for 48 h. The whole process was carried out under hood. Finally, the dried composite powder was fabricated into standard Izod bars via injection molding under the same conditions followed in the fabrication of MM nanocomposites.

Characterization of nc Fe₄₀Ni₆₀ particles

X-ray diffraction (XRD) was employed to characterize the crystallographic texture and crystal size of the synthesized Fe-Ni alloy. XRD measurements were carried out on a Shimadzu XRD-7000 diffractometer (30 kV, 30 mA; Cu K α + Ni-filtered radiation, $\lambda=0.15406$ nm). The 2θ range was 30–110°, at a scanning rate of 4°/min and a scanning step of 0.018°. Chemical composition was estimated by an area analysis using energy dispersive X-ray spectroscopy (EDS) equipped with the scanning electron microscope (SEM, JEOL, Model JSM 6360 LA). The morphology and particle size were analyzed by a field emission scanning electron microscope (Zeiss Ultra-60 FE-SEM), operating at 5 kV. The SEM samples were prepared by dropping a diluted dispersion of Fe-Ni particles onto a silicon wafer and letting the solvent to evaporate.

Characterization of Fe₄₀Ni₆₀/PA6 nanocomposites

Flexural test was performed using a MTS 810 testing machine (MTS Systems Corporation), according to ASTM-D790. Notched Izod impact strength was determined using a CS-137-083 impact tester (Custom Scientific Instruments, INC), according to ASTM-D256. All the tests were conducted at ambient temperature and the reported results reflect an average of three measurements. Thermomechanical properties, including storage modulus and loss tangent ($\tan \delta$), were characterized using dynamic-mechanical analyzer (DMA Q800, TA instruments). The properties were characterized as a function of temperature using a single cantilever mode applying constant strain. The strain amplitude was 0.15 %, the frequency 1 Hz and the heating rate was 3 °C/min. Measurements were performed in the temperature interval 25–180 °C. The presented data are the average of three measurements.

The degree of agglomeration and distribution of nc Fe₄₀Ni₆₀ particles in PA6 matrix were assessed through SEM examination of the impact fracture surface using Zeiss Ultra-60 FE-SEM operating at accelerating voltage of 5 kV. The specimens were gold coated using a Desk IV Sputter/Etch Unit (DENTON Vacuum, LLC).

Modulated differential scanning calorimeter (MDSC Q200, TA instruments) was used to determine the degree of crystallinity and analyze the melting and crystallization behaviors of neat PA6 and PA6 phase in the nanocomposites. The samples of 7 mg were heated from ambient temperature to 270 °C, held at this temperature for 3 min to erase the thermal history and then cooled to 25 °C. All MDSC runs were conducted under nitrogen atmosphere with heating/cooling rates of 5 °C/min. The degree of crystallinity, X_C , was calculated from the enthalpy evolved during melting based on the heating scans, using the following formula [21]:

$$X_C = \frac{\Delta H_m}{(1 - \varnothing)\Delta H_m^0} \times 100 \quad (1)$$

Where ΔH_m is the apparent enthalpy of melting of sample, ΔH_m^0 is the extrapolated value of the enthalpy corresponding to the melting of 100 % crystalline pure PA6, which is taken as 190 J/g [22], and \varnothing is weight fraction of nc Fe₄₀Ni₆₀ in the composites.

XRD was employed to determine the relative fraction of α and γ crystalline phases in neat PA6 and PA6 phase within the nanocomposites. XRD patterns were obtained using X'Pert PRO MPD diffractometer in reflection mode (45 kV, 40 mA; Cu K α + Ni-filtered radiation, $\lambda=0.154$ nm). The analysis was performed on the injection molded Izod bars, at ambient temperature with a 2θ range between 8 and 80°, at a scanning rate of 4°/min and a scanning step of 0.016°. Samples were then heated gradually to 60, 90, 120, 150 and 180 °C and held at each temperature for 5 min before commencing the data collection. The range of 2θ measurement was 8–30° at the same scanning rate and step.

XRD traces were de-convolved to diffraction peaks corresponding to amorphous phase and crystalline phase which is composed of α and γ crystal forms, using MDI Jad9 software. The percentage of γ -phase with respect to the total crystalline phase was calculated by:

$$\gamma(\%) = \frac{A_\gamma}{A_\alpha + A_\gamma} \times 100 \quad (2)$$

Where A_α is the area under α diffraction peaks and A_γ is the area under γ diffraction peaks [23]. In order to check the influence of high temperature processing on the nanostructure of nc Fe₄₀Ni₆₀ alloy, crystallite sizes of nc Fe₄₀Ni₆₀ particles in the nanocomposites were also determined.

Results and discussion

Characteristics of nc Fe₄₀Ni₆₀ particles

Figure 1 shows the XRD pattern of the chemically synthesized particles. The four characteristic peaks for the disordered FCC

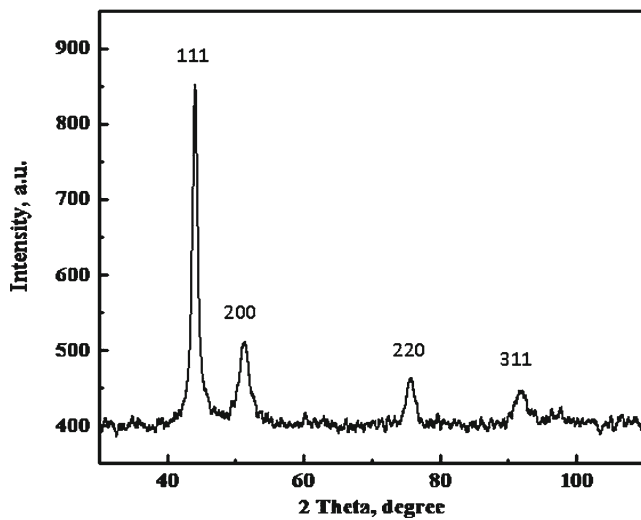


Fig. 1 XRD pattern of the chemically synthesized black particles

γ -Fe-Ni taenite phase ($2\theta=44.05^\circ$, 51.3° , 75.6° and 91.5°), marked by Miller indices ((111), (200), (220) and (311)) are observed [13, 24]. This reveals that the synthesized particles are pure Fe-Ni alloy. The average crystallite size of the synthesized alloy, based on the full width at half maximum of the (111) peak using Scherrer formula [25], is 11 nm. According to EDS quantitative analysis the alloy composition is 36 at.% Fe and 64 at.% Ni, excluding the other elements like carbon in the supporting film and oxygen in the oxide layer formed on the particle surface. Additionally, the oxygen content is only 6 at.%, indicating that the oxide layer formed on particle surface is very thin. The SEM image, presented in Fig. 2, shows that the produced $\text{Fe}_{40}\text{Ni}_{60}$ alloy is composed of spherical particles with a mean diameter of about 150 nm. This suggests that each spherical particle is nanostructured, i.e. it is composed of several nanocrystallites, as previously reported [13, 24]. Based on XRD, EDS and FE-SEM results, it is concluded that the chemically synthesized black particles are nc $\text{Fe}_{40}\text{Ni}_{60}$ submicron sized particles.

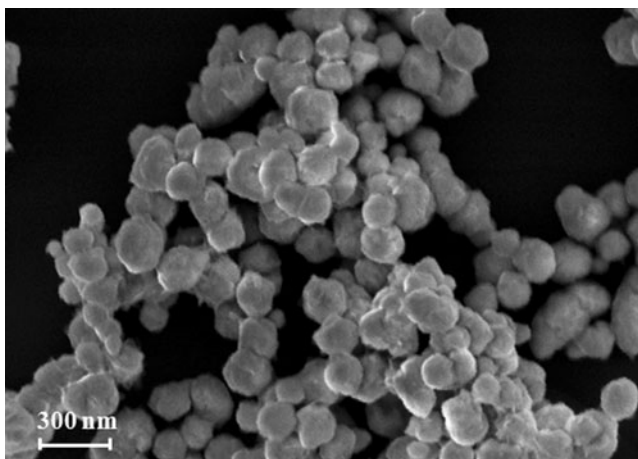


Fig. 2 SEM image of the nc $\text{Fe}_{40}\text{Ni}_{60}$ alloy particles

Mechanical and thermomechanical properties of $\text{Fe}_{40}\text{Ni}_{60}/\text{PA6}$ nanocomposites

Figure 3 shows the flexural modulus and strength of MM and SM composites as a function of nc $\text{Fe}_{40}\text{Ni}_{60}$ content. Regardless of the nanofiller content, SM composites acquire much higher modulus and strength than the corresponding MM composites. This can be attributed to the intensive mixing applied during solution mixing which broke up particle agglomerates and improved the distribution of alloy particles within the polymer matrix as indicated also by SEM. Improved distribution of particles or particle agglomerates and smaller agglomerates result in stronger filler-matrix interactions and thus more efficient stress transfer between the two phases. Figure 3 also indicates that addition of nc $\text{Fe}_{40}\text{Ni}_{60}$ particles to PA6 significantly enhances the modulus and strength in case of SM composites especially for low nanofiller content. The maximum improvement observed is 35 % (modulus) and 26 % (strength), at 3 wt% nc $\text{Fe}_{40}\text{Ni}_{60}$.

It is worth mentioning that although melt mixing usually results in polymer nanocomposites with reasonable mechanical performance [26], in this study the MM composites except MM1, which has comparable modulus and strength to neat PA6, exhibit lower modulus and strength compared to those of neat PA6. This implies that the interfacial adhesion between filler agglomerates and PA6 matrix is very poor and overrides the reinforcing action of the nanofiller, leading to mechanical property deterioration. This is mainly because the supermagnetic Fe-Ni alloy has a strong agglomeration tendency, which couldn't be overcome by the weak forces, applied in MM process.

The impact strength of $\text{Fe}_{40}\text{Ni}_{60}/\text{PA6}$ nanocomposites as a function of the nanofiller loading and compounding method is presented in Fig. 4. Again the SM composites possess much higher impact strength than the corresponding MM

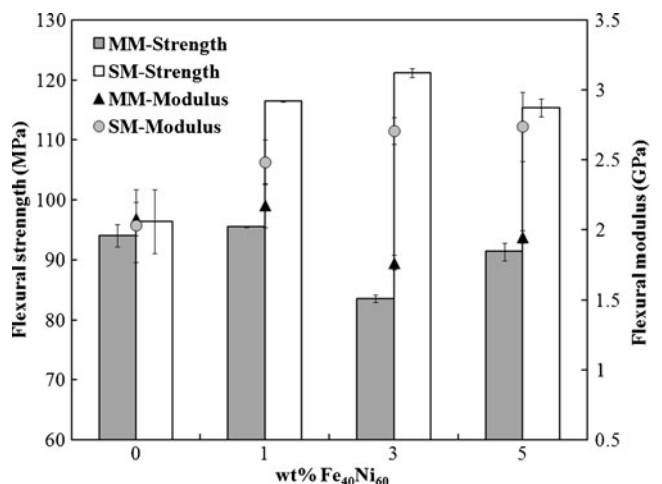


Fig. 3 Flexural properties of $\text{Fe}_{40}\text{Ni}_{60}/\text{PA6}$ nanocomposites as a function of particle content

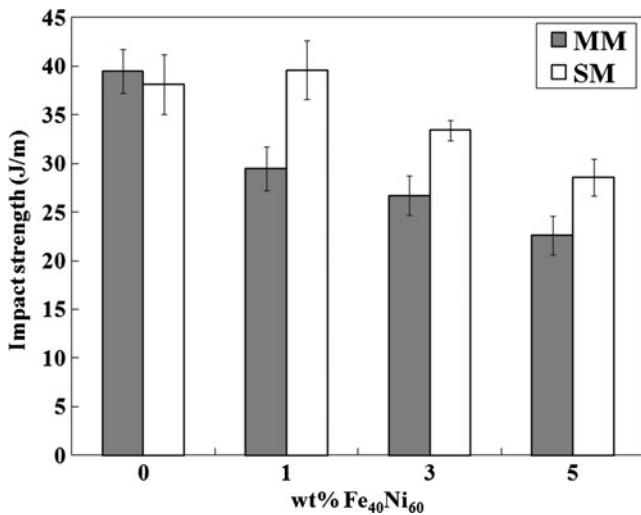


Fig. 4 Impact strength of Fe₄₀Ni₆₀/PA6 nanocomposites as a function of particle content

composites do. However, both composites exhibit lower impact strength compared to that of the neat PA6. The decrease in impact strength becomes more pronounced at higher particle loading. This may be because i) addition of nc Fe₄₀Ni₆₀ particles to PA6 boosts its hardness and stiffness which, in turn, reduces toughness or/and ii) the increased particle agglomeration and agglomerate size at higher filler content, as confirmed by SEM, act as crack nucleation sites [27].

The storage modulus and tan-δ of MM and SM composites as a function of temperature at various nanofiller loadings are shown in Fig. 5a and b, respectively. As indicated the SM composites have higher storage modulus than the MM composites throughout the tested temperature range and both composite systems exhibit higher modulus compared to that of the neat PA6. In addition, the tan-δ of SM composites is significantly lower than that of MM composites in the low 25 °C to 55 °C temperature range, indicating that SM composites are more elastic and can store more energy than the MM composites. It is also noted that the storage modulus is enhanced as the nanofiller content increases in SM composites. Thus, SM5 shows the maximum improvement in storage modulus, 23 %, at ambient temperature. On the other hand, the SM composites have significantly lower tan-δ than neat PA6 (SM0) in the low temperature range from 25 °C to 45 °C. This indicates that as the nanofiller content increases, the load bearing capacity is significantly improved while the dissipated energy is decreased during dynamic deformation of nanocomposites.

The maximum of tan δ is associated with the α-transition (glass transition) of PA6. For SM samples, the temperature of α-peak (glass transition temperature, T_g) increases from 60.5 to 66.2 °C with increasing the particle content from 0 to 5 wt%. As reported in [28], an increase in the T_g of polymer upon addition of a reinforcing nano-filler is an evidence for

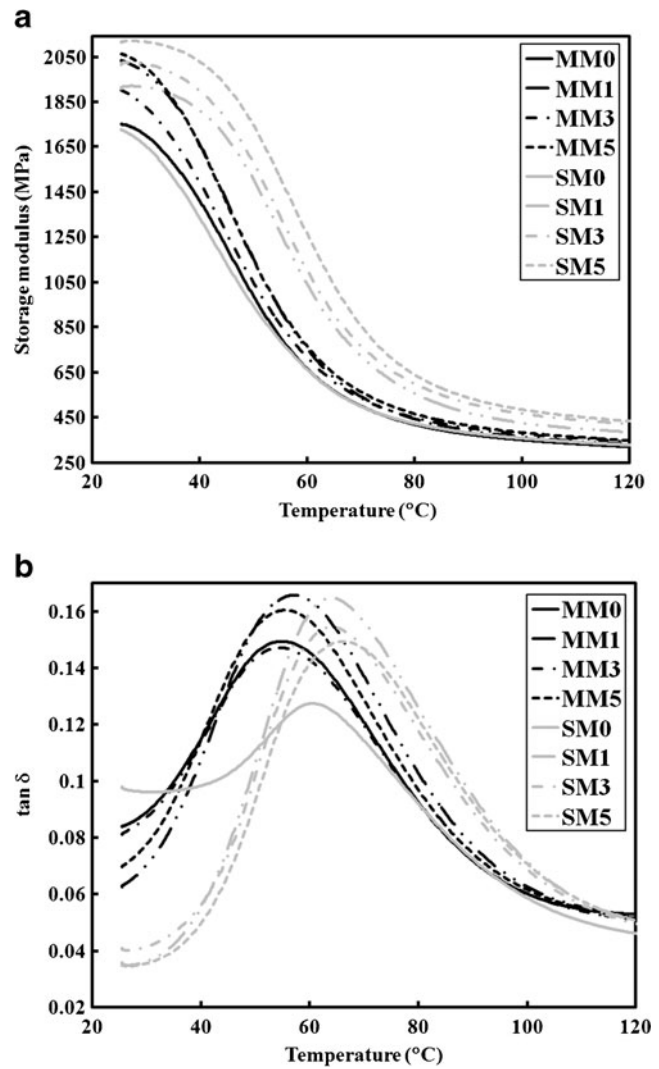


Fig. 5 Thermomechanical properties of Fe₄₀Ni₆₀/PA6 nanocomposites as a function of temperature at various nc Fe₄₀Ni₆₀ content. **a** Storage modulus, **(b)** tan-δ

the good distribution of filler within polymer matrix. This suggests that nc Fe₄₀Ni₆₀ particles exhibit good distribution in PA6 matrix, causing severe constraint on the polymer segmental motion, so that, the transition from glassy state to rubbery state occurs at higher temperature. In case of MM composites the T_g of PA6 is slightly shifted to higher temperature upon addition of 1 wt% nc Fe₄₀Ni₆₀ particles. Whereas, further increase of particle loading causes T_g to decrease again, which reveals that nanofiller does not affect polymer chain mobility. This may be due to the presence of agglomerates and poor distribution within polymer matrix which decrease the nc Fe₄₀Ni₆₀-particles/polymer contact area and interactions.

Restriction of polymer chain mobility that is evidenced by increased T_g of PA6 matrix in SM composites, contributes to the enhancement of storage modulus, flexural modulus and

strength and the decreased impact strength of these nanocomposites compared to the properties of neat PA6.

Morphology of Fe₄₀Ni₆₀/PA6 nanocomposites

SEM micrographs of MM and SM composites are presented in Fig. 6. It is referred to some of nc Fe₄₀Ni₆₀ particles, appeared in the micrographs, by arrows in order to clearly indicate them. For MM composites, it is obvious that nanoparticle agglomeration is predominant, the degree of agglomeration is more pronounced and the agglomerate size increases at larger filler content. Furthermore, the agglomerates are not uniformly distributed within the PA6 matrix. Such morphology limits the filler-matrix contact area which, in turn, results in poor interfacial interactions and therefore insufficient stress transfer between the two phases, leading to poor mechanical and thermomechanical properties. Unlike MM composites, SEM micrographs of SM composites reveal fewer nc Fe₄₀Ni₆₀ agglomerates that are better distributed within the PA6 matrix. As expected, the degree of agglomeration increases with the particle content as shown in the micrograph of SM5. This observation is in agreement with the trend found for the flexural properties of the SM composites.

The number average particle sizes (PS) of nc Fe₄₀Ni₆₀ particles in MM and SM composites have been calculated by individual measurement of about 50 particles from SEM micrographs of each composite, using SmartTiff software. In addition the particle-size distribution histograms have been produced using Matlab[®], to provide quantitative assessment of the degree of agglomeration of alloy particles within composites. The PS data reveal that the particle size is much greater for MM samples. Moreover, representative particle-size distribution histograms for MM1, Fig. 7a, and

SM1, Fig. 7b, clearly show that the number of small nanoparticles is higher in the SM1 composite whereas the MM1 composite contains larger number of agglomerates and exhibits a broader size distribution. Obviously, the average particle sizes of nc Fe₄₀Ni₆₀ particles within SM composites are significantly smaller than that estimated from the SEM image of the chemically synthesized alloy powder, Fig. 2. This confirms that the intensive mixing applied during solution mixing broke up the submicron supermagnetic agglomerates into smaller nanoparticles.

Crystalline structure of Fe₄₀Ni₆₀/PA6 nanocomposites

Figure 8 illustrates the MDSC heating scans for MM, SM composites and the corresponding PA6 controls. Upon heating from 40 to 270 °C, a small exothermic peak, around 189 °C for MM composites and 195 °C for SM composites, followed by a sharp endothermic peak around 222 °C were observed for all samples. This endothermic peak is mainly associated with the melting of α -form crystals of PA6 [29]. However, the presence of a long tail at the beginning of peak reveals that there is a fraction of γ -form crystals which usually melt around 210 °C [30]. The sub-T_m exotherm in nylons is attributed to the release of strain energy absorbed during processing [31].

The degree of crystallinity, melting and crystallization temperatures of PA6 matrix in MM and SM composites are listed in Table 2. For MM composites, it is evident that the degree of crystallinity, melting and crystallization temperatures of PA6 are insensitive to the presence of nc Fe₄₀Ni₆₀ particles, at all nanofiller loadings used in the study. On contrary all SM composites have significantly higher degree of crystallinity and crystallization temperature than neat PA6. The increased crystallization temperatures of PA6 phases in such composites

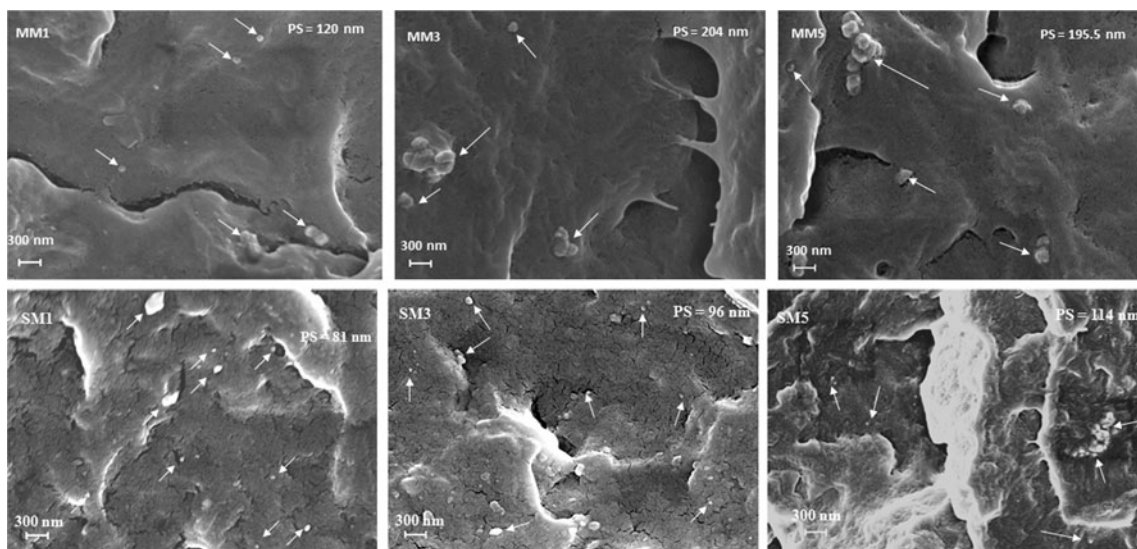


Fig. 6 SEM micrographs of Fe₄₀Ni₆₀/PA6 nanocomposites

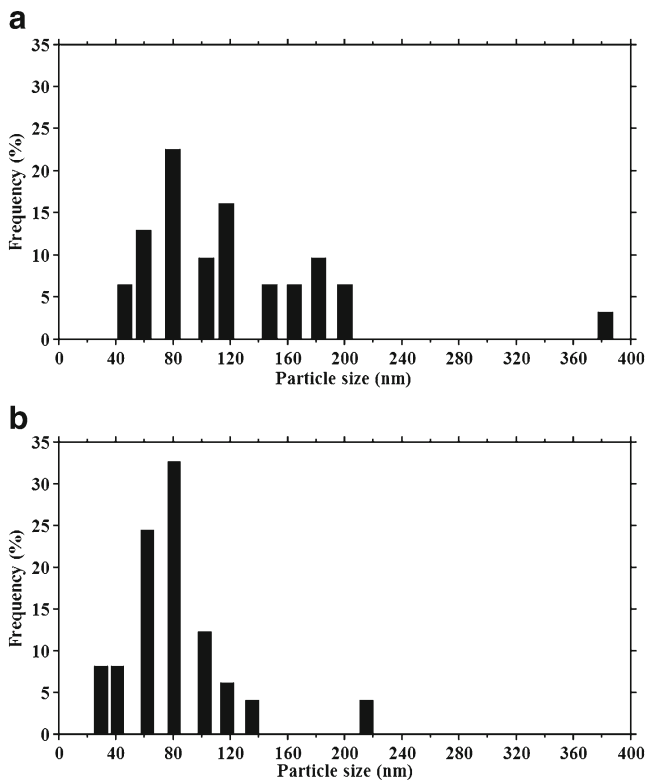


Fig. 7 Particle-size distributions histogram of nc Fe₄₀Ni₆₀ particles in (a) MM1 and (b) SM1

indicate that the nc Fe₄₀Ni₆₀ particles act as effective nucleating agent, thus allowing the crystallization of PA6 molecules to start earlier and inducing the rate of crystallization that eventually leads to increased degree of crystallinity. Conversely, the increased restriction of PA6 chain mobility with the increase of nanofiller content, as revealed from T_g values, hinders the crystallization of PA6 molecules and as a consequence lowers the degree of crystallinity. These counteracting effects of nc Fe₄₀Ni₆₀ particles interpret why the increase in

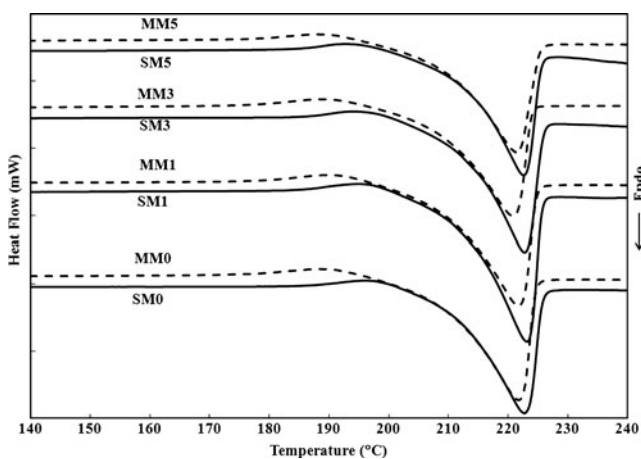


Fig. 8 MDSC heating traces of Fe₄₀Ni₆₀/PA6 nanocomposites

Table 2 DSC data for MM and SM composites

Sample	Xc	T _m (°C)	T _c (°C)
MM0	37	222	194
MM1	37	222	194.5
MM3	38	221	194.5
MM5	38	221.5	194.5
SM0	34	223	195.5
SM1	39.5	223	197.5
SM3	38	223	197
SM5	36	223	197

the degree of crystallinity of PA6 phase over that of neat PA6, exhibits maximum at 1 wt% nc Fe₄₀Ni₆₀ then decreases as the nanofiller content increases within SM composites. Unlike the degree of crystallinity and crystallization temperature, no significant change in the melting temperature with the nanofiller content is observed, revealing that the size and perfection of PA6 crystals appear unaffected by the increase of nanofiller content in SM composites.

XRD patterns for MM, SM composites and the corresponding PA6 controls are presented in Fig. 9. The peaks around 2θ ≈ 20° and 23° are assigned to α₁ and α₂ crystal planes of PA6, respectively. While the peaks around 2θ ≈ 10°, that appears only in the XRD scan of SM5, and 21° are assigned to γ₁ and γ₂ crystal planes of PA6, respectively [29]. The observed peaks around (2θ=44°, 51°, 75°) are attributed to the disordered FCC γ-Fe-Ni taenite phase, as mentioned before. γ-phase (%) and crystallite sizes of nc Fe₄₀Ni₆₀ in MM, SM composites and the corresponding neat PA6 controls are listed in Table 3. Clearly, the α-form is predominant in both neat PA6 controls and MM composites. Presence of nc Fe₄₀Ni₆₀ particles has a negligible effect on the polymorphic crystalline structure of PA6 in MM composites (the γ-phase (%) in MM3 and MM5 is slightly

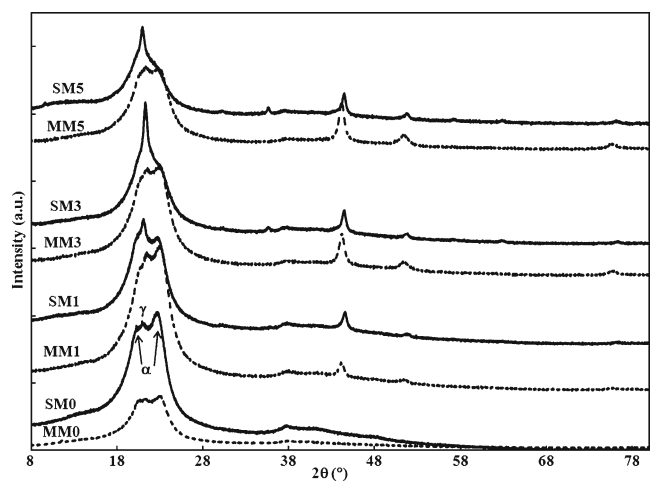


Fig. 9 XRD patterns of Fe₄₀Ni₆₀/PA6 nanocomposites

Table 3 XRD data for MM and SM composites

Sample	γ (%)	Crystallite size of Fe ₄₀ Ni ₆₀ (nm)
Fe ₄₀ Ni ₆₀ nanoparticles		11
MM0	35.5	
MM1	35.5	13.5
MM3	40	12.5
MM5	39.5	12.5
SM0	38	
SM1	48	15
SM3	63	15
SM5	66	15.5

higher than that in MM0), which is in agreement with DSC results. This reveals that the crystallization of PA6 phase is insensitive to the presence of nc Fe₄₀Ni₆₀ particles in MM composites, owing to large particle agglomeration and poor distribution which minimize the filler-matrix interactions. Conversely, the relative fraction of γ -form to α -form crystals significantly increases as the nanofiller content increases in SM composites and γ -form becomes predominant in SM3 and SM5. Based on the discussion reported in previous researches which studied the crystallization of clay/PA6 [23] and MWNTs/PA6 nanocomposites [17], it is speculated that

the possible reasons of this phenomenon are: a) nc Fe₄₀Ni₆₀ particles constrain the mobility of PA6 molecules, and as a result, chain packing into well ordered crystals becomes more difficult than in neat PA6. Therefore, the less ordered γ -crystal form is favored in the presence of nc Fe₄₀Ni₆₀ particles; b) as the size of the good distributed nc Fe₄₀Ni₆₀ particles within PA6 phase is somewhat large, the filler particles disturb the PA6 crystals while being formed during the crystallization process, leading to the profusion of less ordered γ -phase crystals in SM composites as compared to neat PA6. The significant effect of nc Fe₄₀Ni₆₀ particles on the crystallization of PA6, as revealed from DSC and XRD analyses, can be considered as evidence for the good interfacial interaction between nc Fe₄₀Ni₆₀ particles and PA6 in SM composites.

XRD traces at high temperatures indicate that the relative fraction of γ -form to α -form crystals in neat PA6 control and SM composites increases by increasing temperature up to 120 °C. Further increase in temperature, however, results in reconversion of γ -form crystals to α -form crystals and α -phase become predominant at 180 °C. This explains why melting peak in the DSC thermograms is mainly associated to α -form crystals, although, γ phase is predominant in SM composites at ambient temperature.

The increased degree of crystallinity of PA6 phase in SM composites is a possible reinforcing mechanism that

Table 4 Relative mechanical and thermomechanical properties of Fe₄₀Ni₆₀/PA6 nanocomposites made by SM and previously studied PA6 nanocomposites

Ref. no.	Nanofiller	Filler content (wt%)	Composite preparation method	Relative flexural modulus	Relative flexural strength	Relative impact strength	Relative storage modulus
Clay/PA6 nanocomposites							
[32]	p-Silicate nanotubes of the mineral halloysite	10	Direct melt mixing followed by injection molding	-	-	-	1.07
		20		1.1			
		30		1.15			
[33]	Octadecylammonium-treated montmorillonite	4		1.38	1.11	-	1.13
[34]	Sondium Saponite Cation exchange capacity of 71.2 meq/100 g clay	2.5	In-situ polymerization followed by molding	1.13	-	0.98	-
		5		1.24	0.95		
CNT's/PA6 nanocomposites							
[35]	p-MWNTs	2	Master batch technique	1.12	1.09	-	-
		4		1.19	1.16		
[36]	Hexadecylamine functionalized MWCNTs	1	Direct melt mixing followed by molding	-	-	-	1.22
Silica/PA6 nanocomposite							
[37]	p-nanosilica	4.3	In-situ polymerization followed molding	-	-	0.5	1.18
	γ -glycidoxypropyltrimethoxysilane treated nanosilica	4.3		-	-	1.26	1
Fe ₄₀ Ni ₆₀ /PA6 nanocomposite							
	p-nc Fe ₄₀ Ni ₆₀ particles	1	Solution mixing followed by molding	1.22	1.21	1.04	1.11
		3		1.33	1.26	0.874	1.17
		5		1.35	1.20	0.75	1.23

contributes to the increased storage modulus, flexural modulus and strength but lower impact strength of such composites as compared to neat PA6. Damping in the increased degree of crystallinity and increase of the relative fraction of γ -form to α -form crystals, however, lead to the reduced rate at which the storage modulus, flexural modulus and strength are enhanced with the increase of the nanofiller content in SM nanocomposites. The later factor is also responsible for the significantly higher impact strength of SM composites compared to that of the corresponding MM ones.

On the other hand, Table 3 shows that crystallite sizes of nc Fe₄₀Ni₆₀ particles in both MM and SM composites are slightly larger than that of the as synthesized alloy powder. This indicates that there is small Fe₄₀Ni₆₀ crystal growth due to the thermal energy applied during composites processing. The phenomenon is more obvious in SM composites where the composite powder tends to sinter when subjected to heat during feeding into extruder, forming large aggregates. Feeding of these composite aggregates into extruder was very difficult and slow, leading to more crystal growth and little extent of oxidation of nc Fe₄₀Ni₆₀ particles. Oxidation of small portion of nc Fe₄₀Ni₆₀ particles is evidenced from the very weak magnetite peak ($2\theta=35.6^\circ$) [13], that appears in XRD traces of SM3 and SM5.

Finally, the relative mechanical and thermomechanical properties of SM composites are compared with those of previously investigated clay, carbon nanotubes (CNT's) and silica reinforced PA6 nanocomposites for evaluating the novel Fe-Ni alloy/PA6 nanocomposite among the currently existing PA6 nanocomposites. The data are illustrated in Table 4. The preparation method of composites and whether the reinforcing nanofiller is pristine (p-) or functionalized with polar molecules, are indicated. This is because; these two parameters significantly affect the morphology, crystalline structure and therefore the overall performance of PA6 nanocomposites. Clearly, that the performance of p-Fe₄₀Ni₆₀/PA6 nanocomposites made by SM is in general good as well as those of other PA6 nanocomposites, indicating that this new nanocomposite is promising. The performance can be further significantly improved by minimizing particle agglomeration and improving the interfacial adhesion between metallic nanofiller and PA6 matrix through functionalization of alloy particles with polar molecules, utilizing ultrasound power during nanocomposite preparation or preparation of nanocomposite by in-situ method. Thereby, Fe₄₀Ni₆₀/PA6 nanocomposite will be potential candidate material for engineering applications.

Conclusions

Fe₄₀Ni₆₀/PA6 nanocomposites were fabricated using two different compounding processes and their properties were

characterized as a function of the compounding method and nanofiller content. Structural analyses including SEM, DSC and XRD reveal that there is good interfacial interaction between nanofiller particles and PA6 in SM composites but not in MM ones. Thus, the improved distribution of particles, presence of fewer and smaller particle agglomerates, increased crystallinity and T_g counteract the growth of γ -crystal form and the net result is significant enhancement of storage modulus, flexural modulus and strength of SM composites over neat PA6 and MM composites. However, larger particle size, worse distribution of particles, damping in the increased degree of crystallinity and growth of the relative fraction of γ -form to α -form crystals interpret the reduced rate of enhancement of such properties with the increase of nanofiller content in SM composites. The impact strength of SM composites is remarkably higher than MM composites but, unlike other properties, is less than that of neat PA6 because increased crystallinity and T_g diminish the toughness.

Considering the mechanical and thermomechanical properties, it is concluded that 3 wt% nc Fe₄₀Ni₆₀/PA6 composite made by SM is the composite with the optimum overall performance. Thus, compared to the previously investigated PA6 nanocomposites reinforced with other fillers, SM3 can be a good candidate material for engineering applications.

Acknowledgments The authors deeply appreciate the financial support (Ph.D. scholarship 51218) by the Egyptian Ministry for High Education and Scientific Research. Special thanks to Custom Resins, Inc, USA for supplying PA6, and Prof. Satish Kumar, School of Materials Science and Engineering at Georgia Institute of Technology, for facilitating DSC analysis. We wish to thank Anastasios Patsidis, Mehdi Karvan and Md Bhuiyan, Ph.D. students, School of Mechanical Engineering at Georgia institute of Technology, from Georgia Institute of Technology, for their kind assistance throughout the experimental work.

References

1. Mai Y-W, Yu Z-Z (2006) Polymer nanocomposites. Woodhead Publishing Limited, Cambridge
2. Song HM, Kim YJ, Park JH (2008) Three-dimensional hierarchically organized magnetic nanoparticle polymer composites: achievement of monodispersity and enhanced tensile strength. *J Phys Chem C* 112:5397–5404
3. Liang Y, Xia X, Luo Y, Jia Z (2007) Synthesis and performances of Fe₂O₃/PA-6 nanocomposite fiber. *Mater Lett* 61:3269–3272
4. Mallakpour S, Zeraatpisheh F (2012) Preparation and morphology distinguishing of novel ZnO ultrafine particle filled nanocomposites contain new poly(amide-imide) via ultrasonic process. *J Polym Res* 19:9927–9936
5. Laachachi A, Cochez M, Ferriol M, Lopez Cuesta JM, Leroy E (2005) Influence of TiO₂ and Fe₂O₃ fillers on the thermal properties of polymethyl methacrylate (PMMA). *Mater Lett* 59:36–39
6. Althues H, Henle J, Kaskel S (2007) Functional inorganic nanofillers for transparent polymers. *Chem Soc Rev* 36:1454–1465

7. Balazs AC, Emrick T, Russell TP (2006) Nanoparticle polymer composites: where two small worlds meet. *Science* 314:1107–1110
8. Chu J-W, Shim I-W (1993) The chemistry of ruthenium in cellulose acetate: reactions with CO, H₂, O₂ and H₂O. *J Mol Catal* 78:189–199
9. Mathiyarasu J, Senthilkumar S, Phani KLN, Yegnaraman V (2008) PEDOT-Au nanocomposite film for electrochemical sensing. *Mater Lett* 62:571–573
10. François NJ, Allo S, Jacobo SE, Daraio ME (2007) Composites of polymeric gels and magnetic nanoparticles: preparation and drug release behavior. *J Appl Polym Sci* 105:647–655
11. Carotenuto G, Martorana B, Perlo P, Nicolais L (2003) A universal method for the synthesis of metal and metal sulfide clusters embedded in polymer matrices. *J Mater Chem* 13:2927–2930
12. Reboud V, Kehagias N, Striccoli M, Placido T, Panniello A, Curri ML, Zelsmann M, Reuther F, Gruetzner G, Torres CMS (2007) Photoluminescence enhancement in metallic nanocomposite printable polymer. *J Vac Sci Technol B* 25:2642–2644
13. Mohamed MA, El-Maghraby AH, Abd El-Latif MM, Farag HA (2013) Optimum synthesis conditions of nanometric Fe₅₀Ni₅₀ alloy formed by chemical reduction in aqueous solution. *B Mater Sci* (in press).
14. Yeh YM, Tu GC, Fang GC (2004) Nanomechanical properties of nanocrystalline Ni-Fe mold insert. *J Alloys Compd* 372:224–230
15. Hamzaoui R, Elkedim O, Gaffet E (2004) Milling conditions effect on structure and magnetic properties of mechanically alloyed Fe-10 % Ni and Fe-20 % Ni alloys. *Mater Sci Eng, A* 381:363–371
16. Li J, Fang Z, Tong L, Gu A, Liu F (2006) Polymorphism of nylon-6 in multiwalled carbon nanotubes/nylon-6 composites. *J Polym Sci Pol Phys* 44:1499–1512
17. Phang IY, Ma J, Shen L, Liu T, Zhang W-D (2006) Crystallization and melting behavior of multi-walled carbon nanotube-reinforced nylon-6 composites. *Polym Int* 55:71–79
18. Shen L, Phang IY, Liu T (2006) Nanoindentation studies on polymorphism of nylon 6. *Polym Test* 25:249–253
19. Nylon 6 (2012) Wikipedia. Nylon 6. http://en.wikipedia.org/wiki/Nylon_6. Accessed 29 July 2012
20. A guide to Nylon (2012) Polymer technology and services, LLC. http://ptslc.com/intro/nylon_intro.aspx. Accessed 29 July 2012
21. Ratna D, Divekar S, Samui AB, Chakraborty BC, Banthia AK (2006) Poly(ethylene oxide)/clay nanocomposite: thermomechanical properties and morphology. *Polym* 47:4068–4074
22. Wu Q, Liu X, Berglund LA (2001) An unusual crystallization behavior in polyamide 6/montmorillonite nanocomposites. *Macromol Rapid Commun* 22:1438–1440
23. Seltzer R, Frontini PM, Mai Y-W (2009) Effect of hygrothermal ageing on morphology and indentation modulus of injection moulded nylon 6/organoclay nanocomposites. *Compos Sci Technol* 69:1093–1100
24. Wei X-W, Zhu G-X, Zhou J-H, Sun H-Q (2006) Solution phase reduction to Fe-Ni alloy nanostructures with tunable shape and size. *Mater Chem Phys* 100:481–485
25. Cullity BD (1956) Elements of x-ray diffraction. Addison-Wesley Publishing Company, Inc
26. Pielichowska K (2012) The influence of molecular weight on the properties of polyacetal/hydroxyapatite nanocomposites. Part 1. Microstructural analysis and phase transition studies. *J Polym Res* 19:9775–9790
27. Chen B, Evans JRG (2009) Impact strength of polymer-clay nanocomposites. *Soft Matter* 5:3572–3584
28. Baji A, Mai Y-W, Wong S-C, Abtahi M, Du X (2010) Mechanical behavior of self-assembled carbon nanotube reinforced nylon 6,6 fibers. *Compos Sci Technol* 70:1401–1409
29. Hu X, Zhao X (2004) Effects of annealing (solid and melt) on the time evolution of polymorphic structure of PA6/silicate nanocomposites. *Polym* 45:3819–3825
30. Xie S, Zhang S, Liu H, Chen G, Feng M, Qin H, Wang F, Yang M (2005) Effects of processing history and annealing on polymorphic structure of nylon6/montmorillonite nanocomposites. *Polym* 46:5417–5427
31. Khanna YP (1992) Overview of transition phenomenon in nylon 6. *Macromolecules* 25:3298–3300
32. Handge UA, Höchstätter KH, Altstädt V (2010) Composites of polyamide 6 and silicate nanotubes of the mineral halloysite: influence of molecular weight on thermal, mechanical and rheological properties. *Polym* 51:2690–2699
33. Chow WS, Mohd Ishak ZA (2007) Mechanical, morphological and rheological properties of polyamide 6/organo-montmorillonite nanocomposites. *eXPRESS Polym Lett* 1:77–83
34. Wu T-M, Chen E-C (2002) Polymorphic behaviour of nylon 6/saponite and nylon 6/montmorillonite nanocomposites. *Polym Eng Sci* 42:1141–1150
35. Shen Z, Bateman S, Wu DY, McMahon P, Olio MD, Gotama J (2009) The effects of carbon nanotubes on mechanical and thermal properties of woven glass fibre reinforced polyamide-6 nanocomposites. *Compos Sci Technol* 69:239–244
36. Liu H, Wang X, Fang P, Wang S, Qi X, Pan C, Xie G, Liew KM (2010) Functionalization of multi-walled carbon nanotubes grafted with self-generated functional groups and their polyamide 6 composites. *Carbon* 48:721–729
37. Li Y, Yu J, Guo Z-X (2002) The influence of silane treatment on nylon 6/nano-SiO₂ in situ polymerization. *J Appl Polym Sci* 84:827–834